Journal of the Korean Physical Society, Vol. 34, No. 1, January 1999, pp. 29∼35

One-Dimensional Analysis of Electronegative Discharge Plasmas with Four Charged Species

H. J. Yoon and T. H. Chung

Department of Physics, Dong-A University, Pusan 604-714s

(Received 23 September 1998)

We develop a parabolic model and a flat-top model for high-density plasma discharges of oxygen gases. These models are based on the equilibrium of a four-species (O_2^+, O^+, O^-, and e) electronegative gas discharge. Such a discharge can consist of an electronegative core and electropositive edge regions, but the electropositive regions become small for the highly electronegative plasma considered here. The approximation of a parabolic or a flat-top negative-ion profile results in algebraic equations which can be solved numerically over a range of parameters. These models consist of the energy and the particle balance equations. For a specified discharge length, absorbed power, and pressure, as well as specified electron temperature-dependent reaction-rate coefficients and surface recombination constants, we solve the energy and the particle balance equations to determine the densities of all species and the electron temperature. The results for typical cases are compared with the experimental data.

I. INTRODUCTION

Electronegative gases have been used in the microelectronics industry for plasma processing steps such as thin-film etching and deposition. However, the gas chemistry of electronegative discharges is pooly understood. The presence of negative ions complicates the discharge phenomena [1]. The number of equations governing the equilibrium is large, and numerical analysis becomes complicated.

There have been many approaches to describe an electronegative plasma. Fluid models have been developed for chlorine gas by Park and Economou [2] and by Sommerer and Kushner [3]. Spatially averaged global models have been developed for various regions of rf discharge plasmas [1,4–8], and analytic equilibrium models have been proposed and compared with experimental results and other simulation results [9–12]. Only a few theoretical analyses of high-density, low-pressure rf and pulsed operation of electronegative discharges have been published. Such analyses may give us a fundamental understanding of the governing precesses and thus help us to design better reactors, to find suitable modulation periods, and to find various suitable operating parameters [13,14]. The one-dimensional equilibrium model gives much simpler equations than do simulation methods such as the particle-in-cell (PIC) model [15] or fluid models [2,3,16]. Moreover, the equations are so simple that the relations between fundamental mechanisms and the resulting plasma parameters become clear.

We are concerned with the equilibrium (steady-state) charged-particle densities. The assumption of a parabolic profile for the negative ions in the electronegative region reduces the problem to a set of coupled algebraic equations from which rather straightforward numerical results can be obtained. In this study, we do not consider either heating mechanisms or sheaths. The equilibrium discharge properties can be combined with the heating and the sheath properties to obtain a complete discharge model [17,18]. Such a complex model does not have completely analytical equilibrium solutions. The plasma is generally divided into two regions, an electronegative (EN) core and an electropositive (EP) edge with a parabolic or a flat-top profile for both the negative and the positive ions, and only half of the plasma is considered because of symmetry. There is also a sheath between the plasma and the external wall or electrode, but we do not consider the details of this region. The EN core consists primarily of positive ions and negative ions, with a smaller component of electrons. The density decreases from the center, and an approximately ambipolar diffusion equation governs the positive-ion diffusion.

Particle balances are written for all species of interest. For the charged-particles, the appropriate ambipolar diffusion rates in the presence of negative ions are used to determine the positive-ion losses. The complete set of equations is solved self-consistently to obtain the concentrations of all species and the electron temperature. The power balance includes energy-loss channels for electron-neutral collisions, dissociation, ionization, dissociative attachment, and electron detachment. In

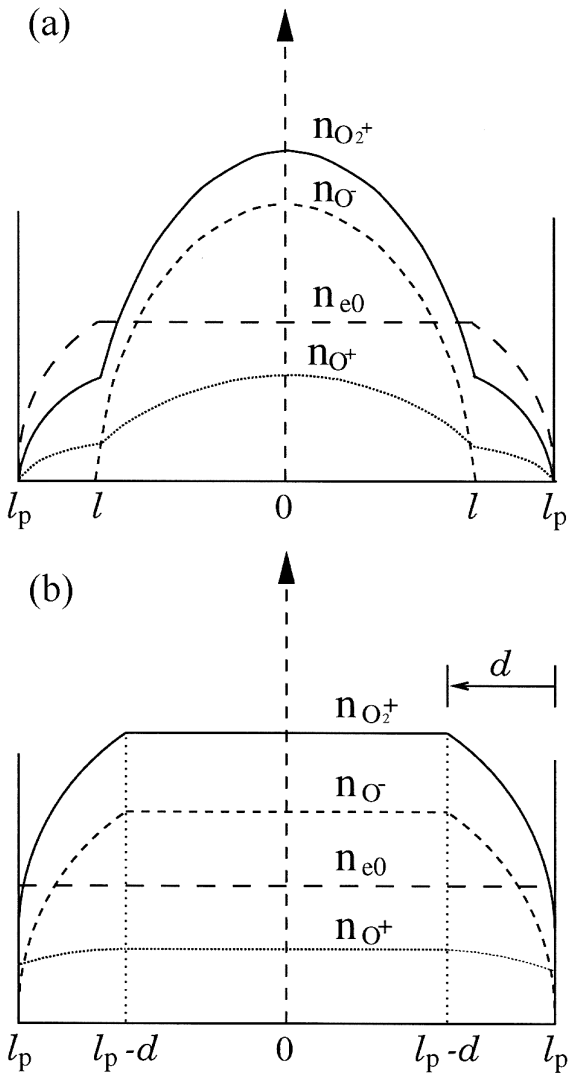

Fig. 1. Density profiles for an electronegative plasma with an electronegative core and an electropositive edge: (a) parabolic model and (b) flat-top model.

addition, energy-loss processes for heavy-particle collisions, such as ion-ion recombination, are included.

The purpose of this work is to calculate the electron density n_e, the negative-ion density n_-, the positive-ion densities ($n_{O_2^+}$ and n_{O^+}), and the atomic and the molecular densities (n_{O_2} and n_O) of electronegative oxygen rf discharges and to investigate the influence of operating parameters (neutral gas pressure, applied power, system size) on the species density. This paper is organized as follows: In Section , a physical model and basic equations are presented. Section presents the results of calculations and discussion, and Section presents the conclusions.

II. PHYSICAL MODEL

The use of an electronegative molecular gas greatly complicates the analysis of the particle and the energy balances in high-density, low-pressure discharges. The discharge can stratify into an electronegative core region surrounded by an electropositive halo region [9]. We consider a cylindrical discharge geometry with a radius of 15.25 cm and a height of 3 cm. This low aspect ratio contributes to a high plasma-production efficiency in that it reduces the ratio of the plasma flux hitting the walls to the plasma flux hitting the wafer. The basic assumptions of the model are as follows: (1) The reactor geometry is cylindrical, which is typical of high-density plasma sources, one-dimensional spatial variations are included, and a steady state is assumed. (2) For an electronegative discharge, as shown in Fig. 2, the electron density n_e is assumed to be uniform throughout the discharge except near the sheath edge. The negative-ion density n_{O^-} is assumed to be parabolic, the positive-ion density is $n_i = n_{O_2^+} + n_{O^+} = n_e + n_{O^-}$, with $n_i = n_e = n_{is}$ at the sheath edge. (3) We neglect the energy losses for the processes of dissociation, attachment, and detachment. (4) We assume that only one type of negative-ion is generated. (5) The neutral gas temperature is assumed to be 600 K.

The reaction set used for O_2 is listed in Table **??**. The types of electron-neutral reactions included are ionization, dissociation, excitation, dissociative excitation, dissociative attachment, and electron detachment. We did not include metastables for the oxygen discharge because metastables were found to be unimportant in contributing to the total positive-ion density [1]. Molecular oxygen is the feed gas into the system. On collision with electrons, the molecules undergo electronic transitions to form O_2^+, O^+, O^-, and e.

We consider a four-species plasma (O_2^+, O^+, O^-, and e) in a pure oxygen discharge. The neutral gas pressure is written as

$$p = Nk_BT_g, \tag{1}$$

where N is the neutral gas ($N = N_{O_2} + N_O$) density, k_B is the Boltzmann constant, and T_g is the gas temperature. We only consider dominant generation and destruction for oxygen atoms:

$$2k_{diss}n_en_{O_2} = O_{loss}n_O \ , \tag{2}$$

where $O_{loss} = \gamma_{rec}\frac{1}{4}\frac{v_{th}A}{V}$ is the oxygen atom loss rate to the wall with $v_{th} = \left(\frac{8k_BT_g}{\pi m_O}\right)^{\frac{1}{2}}$ being the thermal velocity of neutral atoms, and γ_{rec} being the surface recombination rate. Equation (2) becomes

$$2k_{diss}(1-X)n_e = \frac{1}{4}\gamma_{rec}\frac{v_{th}}{L}X \ , \tag{3}$$

where the fractional dissociation X is defined as $\frac{n_O}{n_O+n_{O_2}}$, and L is the system length. Equation (3) gives

$$X = \frac{8n_eLk_{diss}}{8n_eLk_{diss} + \gamma_{rec}v_{th}} \ . \tag{4}$$

Table 1. Model reaction set for an oxygen plasma.

Reaction				Rate Coefficients	Units
Ionization 1	$e + O$	$\rightarrow$	$O^+ + 2e$	$k_{iz1} = 9 \times 10^{-15} T_e{}^{0.7} \exp(-\frac{13.6}{T_e})$	$\mathrm{m^{-3}s^{-1}}$
Ionization 2	$e + O_2$	$\rightarrow$	${O_2}^+ + 2e$	$k_{iz2} = 9 \times 10^{-16} T_e^2 \exp(-\frac{12.6}{T_e})$	$\mathrm{m^{-3}s^{-1}}$
Recombination 1	$O^- + O^+$	$\rightarrow$	$O_2 + O$	$k_{rec1} = 2.5 \times 10^{-13} \left(\frac{300}{T_g}\right)^{0.5}$	$\mathrm{m^{-3}s^{-1}}$
Recombination 2	${O_2}^+ + O^-$	$\rightarrow$	$O_2 + O$	$k_{rec2} = 1.5 \times 10^{-13} \left(\frac{300}{T_g}\right)^{0.5}$	$\mathrm{m^{-3}s^{-1}}$
Dissociative Attachment	$e + O_2$	$\rightarrow$	$O^- + O$	$k_{att} = 8.8 \times 10^{-17} \exp(-\frac{4.4}{T_e})$	$\mathrm{m^{-3}s^{-1}}$
Detachment	$e + O^-$	$\rightarrow$	$O + 2e$	$k_{det} = 2 \times 10^{-13} \exp(-\frac{5.5}{T_e})$	$\mathrm{m^{-3}s^{-1}}$
Dissociation	$e + O_2$	$\rightarrow$	$2O + e$	$k_{diss} = 4.2 \times 10^{-15} \exp(-\frac{5.6}{T_e})$	$\mathrm{m^{-3}s^{-1}}$
Wall Recombination	$O + O$	$\rightarrow$	O_2	$O_{loss} = \gamma_{rec} \frac{1}{4} \frac{v_{th} A}{V}$	$\mathrm{s^{-1}}$

Therefore, the oxygen gas density is:

$$n_{O_2} = (1 - X)N, \tag{5}$$

$$n_O = XN. \tag{6}$$

1. Parabolic Model

From Ref. 10, assuming a parabolic distribution of the negative ions and the positive ions in the electronegative core region and a constant electron density n_{e0}, we have

$$n_{{O_2}^+}(x) = \overline{n_{{O_2}^+}} \left(1 - \frac{x^2}{l^2}\right) + n_{{O_2}^+}(l) \ , \tag{7}$$

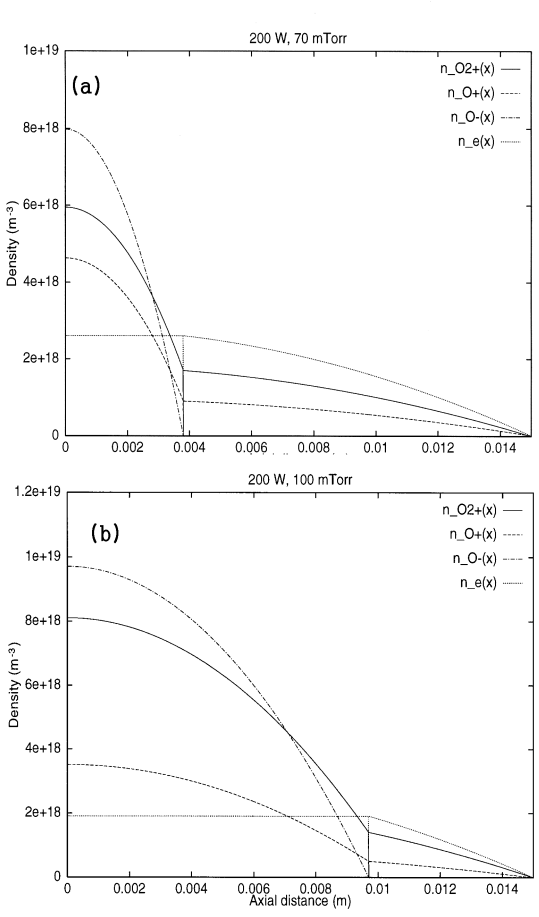

Fig. 2. Density profiles from the parabolic model of the oxygen discharge with four species at an input power of 200 W and a gas pressure of (a) 70 mTorr and (b) 100 mTorr.

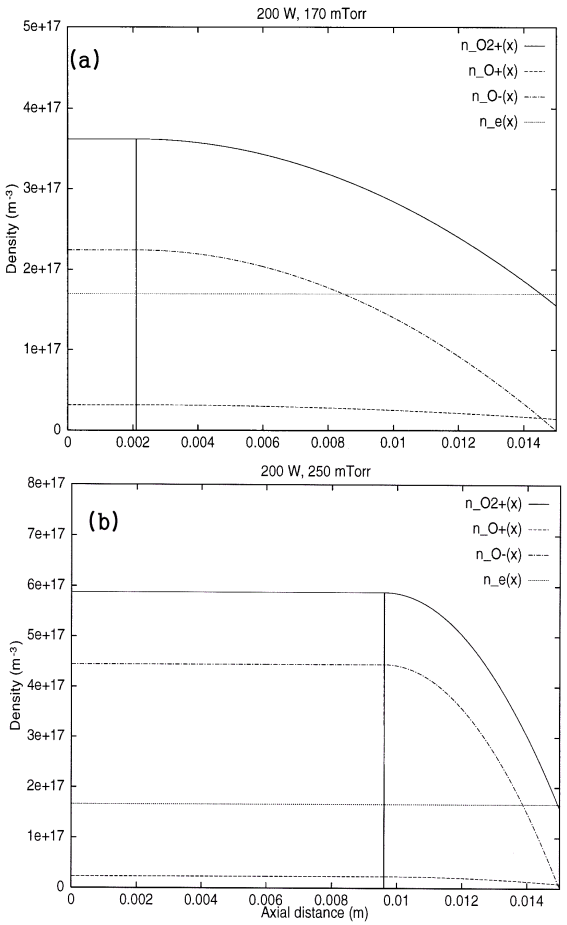

Fig. 3. Density profiles from the flat-top model of the oxygen discharge with four species at an input power of 200 W and a gas pressure of (a) 170 mTorr and (b) 250 mTorr.

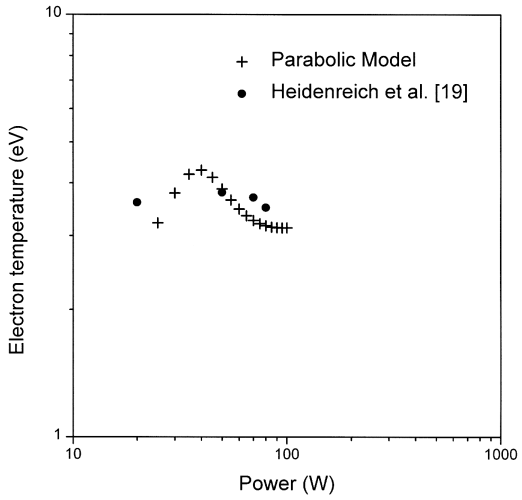

Fig. 4. Comparison of model and experimental data for the variation of the electron temperature with input power. The + signs indicate the calculated result for the experimental setup, and the circles indicate the experimental data.

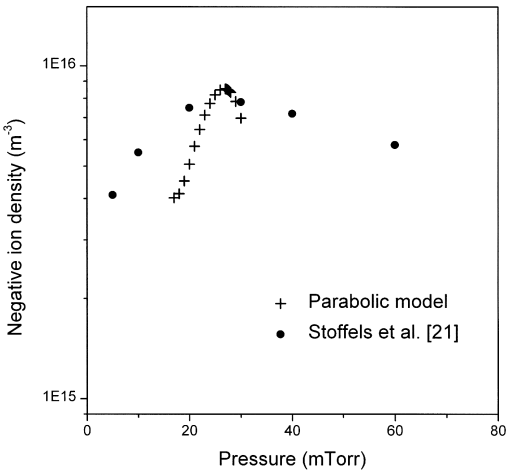

Fig. 6. The measured and calculated negative-ion density. The experimental data are the averaged densities. The calculations were performed at $T_e = 3$ eV. The + signs are the calculated results based on the conditions of the experimental setup, and the circles are the experimental data.

$$n_{O^+}(x) = \overline{n_{O^+}} \left(1 - \frac{x^2}{l^2}\right) + n_{O^+}(l) \ , \tag{8}$$

$$n_-(x) = n_{e0}\alpha_0 \left(1 - \frac{x^2}{l^2}\right) \ , \tag{9}$$

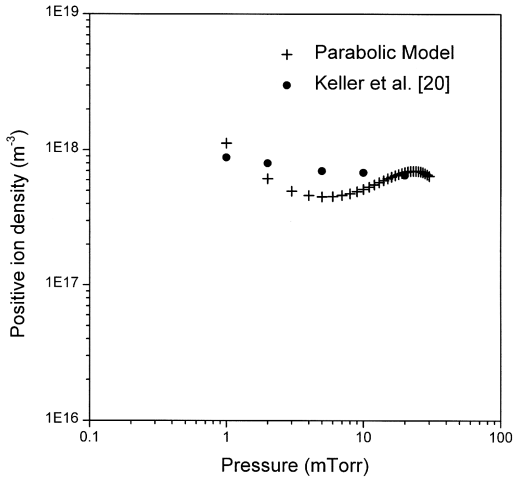

Fig. 5. Total positive-ion density vs. pressure. The + signs are the results calculated based on the conditions of the experimental setup, and the circles are the experimental data.

where α_0 is defined as $\frac{n_{-0}}{n_{e0}}$ and n_{-0} is the negative-ion density at the center of the reactor. These profiles are shown in Fig. 1.(a). The particle-balance equations for the positive ions ($O_2{}^+$ and O^+) at the edge point of the EN core ($x = l$) are

$$\Gamma_{O_2{}^+}(l) = \int_0^l k_{iz2} n_{O_2} n_e dx - \int_0^l k_{rec2} n_{O_2{}^+}(x) n_-(x) dx, \tag{10}$$

$$\Gamma_{O^+}(l) = \int_0^l k_{iz1} n_O n_e dx - \int_0^l k_{rec1} n_{O^+}(x) n_-(x) dx. \tag{11}$$

The particle-balance equation for the negative ions is written as

$$\int_0^{l_p} k_{att} n_{O_2} n_e dx = \int_0^l k_{rec1} n_{O^+}(x) n_-(x) dx + \int_0^l k_{rec2} n_{O_2{}^+}(x) n_-(x) dx + \int_0^l k_{det} n_-(x) n_e dx, \tag{12}$$

where l_p is the half-system length, k_{iz1}, k_{iz2}, k_{att}, k_{rec1}, k_{rec2}, and k_{det} are rate constants for O^+ ionization, $O_2{}^+$ ionization, attachment, O^+ recombination, $O_2{}^+$ recombination, and detachment, respectively. Rewriting Eqs. (10) and (11), we obtain the particle-balance equations for the positive ions:

$$k_{iz2} n_e n_{O_2} l = k_{rec2} \overline{n_{O_2{}^+}} \alpha_0 n_e \left(\frac{8}{15} + \frac{2}{3}\frac{n_{O_2{}^+}(l)}{\overline{n_{O_2{}^+}}}\right) l + \frac{2 D_{aO_2{}^+} \overline{n_{O_2{}^+}}}{l} \ , \tag{13}$$

$$k_{iz1}n_e n_O l = k_{rec1}\overline{n_{O^+}}\alpha_0 n_e\left(\frac{8}{15}+\frac{2}{3}\frac{n_{O^+}(l)}{\overline{n_{O^+}}}\right)l + \frac{2D_{aO^+}\overline{n_{O^+}}}{l} . \quad (14)$$

Rewriting Eq. (12), we can write the negative-ion particle-balance equation as

$$k_{att}n_e n_{O_2} l_p = k_{rec2}\overline{n_{O_2{}^+}}\alpha_0 n_e\left(\frac{8}{15}+\frac{2}{3}\frac{n_{O_2{}^+}(l)}{\overline{n_{O_2{}^+}}}\right)l + k_{rec1}\overline{n_{O^+}}\alpha_0 n_e\left(\frac{8}{15}+\frac{2}{3}\frac{n_{O^+}(l)}{\overline{n_{O^+}}}\right)l+\frac{2}{3}k_{det}\alpha_0 {n_e}^2 l. \quad (15)$$

From charge neutrality we have

$$\overline{n_{O_2{}^+}} + \overline{n_{O^+}} = \alpha_0 n_e . \quad (16)$$

The ion-flux balance equation in the electropositive edge region can be written as

$$\frac{2D_{aO_2{}^+}\overline{n_{O_2{}^+}}}{l} + k_{iz2}n_e n_{O_2}(l_p - l) = h_l n_{O_2{}^+}(l) u_{B_{O_2{}^+}}, \quad (17)$$

$$\frac{2D_{aO^+}\overline{n_{O^+}}}{l} + k_{iz1}n_e n_O(l_p - l) = h_l n_{O^+}(l) u_{B_{O^+}} , \quad (18)$$

where D_{aO^+} and $D_{aO_2{}^+}$ are the ambipolar diffusion coefficients for the O^+ and the ${O_2}^+$ ion over a parabola, respectively, $u_{B_{O^+}}$ and $u_{B_{O_2{}^+}}$ are the Bohm velocities of the oxygen atom and the oxygen molecule respectively, and $h_l = \frac{n_s}{n_{e0}}$ with n_s being the electron density at the plasma edge. The h_l factor is given at low pressures by [10]

$$h_l = \left(\frac{a+\left(\frac{u_{in}}{u_B}\right)^3}{1+a}\right)^{\frac{1}{3}} ,$$
$$u_{in} = \frac{2(D_{aO_2{}^+}\overline{n}_{O_2{}^+} + D_{aO^+}\overline{n}_{O^+})}{l(n_{O_2{}^+}(l) + n_{O^+}(l))}, \quad (19)$$
$$u_B = \frac{u_{BO_2{}^+} + u_{BO^+}}{2},$$

where u_{in} is the ion velocity leaving the electronegative core region and $a = \frac{2}{\pi}\frac{\nu_{iz2}\lambda_2+\nu_{iz1}\lambda_1}{u_{B_{O^+}}+u_{B_{O_2{}^+}}}$ with ν_{iz1} being equal to $k_{iz1}n_O$, ν_{iz2} being equal to $k_{iz2}n_{O_2}$, λ_1 being the ion mean-free path of O^+, and λ_2 being the ion mean free-path of ${O_2}^+$.

The energy-balance equation can be written as

$$P_{abs} = \left(k_{iz2}\varepsilon_{c2}n_e n_{O_2} + k_{iz1}\varepsilon_{c1}n_e n_O\right)V + h_l\left(n_{O_2{}^+}(l)u_{BO_2{}^+} + n_{O^+}(l)u_{BO^+}\right)(\varepsilon_e+\varepsilon_i)A , \quad (20)$$

where $A = 2\pi R^2 + 2\pi RL$ (chamber sufrace area) and $V = \pi R^2 L$ (chamber volume). For charge neutrality, we also have

$$n_{O_2{}^+}(l) + n_{O^+}(l) = n_e . \quad (21)$$

The collisional energy loss can be expressed as

$$K_{iz2}\varepsilon_{c2} = K_{iz2}\varepsilon_{iz2} + K_{exc2}\varepsilon_{exc2} + K_{el2}\varepsilon_{el2} ,$$
$$K_{iz1}\varepsilon_{c1} = K_{iz1}\varepsilon_{iz1} + K_{exc1}\varepsilon_{exc1} + K_{el1}\varepsilon_{el1} , \quad (22)$$

where the ε_j terms are the threshold energies required for the processes of ionization, excitation, and elastic collision. The energies of the escaping ions and electrons and the plasma potential are

$$\varepsilon_i = \frac{T_e}{2} + V_s, \quad \varepsilon_e = 2T_e, \quad V_s = \frac{T_e}{2}\ln\left(\frac{M_{O_2}}{2\pi m}\right) . \quad (23)$$

We assume that the density profiles of the positive ions in the electropositive edge region are

$$n_{O_2{}^+}(x) = n_2\left(1 - \frac{x^2}{{l_2}^2}\right) , \quad (24)$$

$$n_{O^+}(x) = n_1\left(1 - \frac{x^2}{{l_1}^2}\right) . \quad (25)$$

At $x = l_p$ (near the reactor wall), the positive-ion (${O_2}^+$) flux balance is written as

$$\Gamma_{O_2{}^+}(x = l_p) = -D_{aO_2{}^+}\frac{n_{O_2{}^+}(x)}{dx}\Big|_{x=l_p} = n_{O_2{}^+}(x = l_p)u_{BO_2{}^+} . \quad (26)$$

Then, from Eqs. (24) and (26), we find

$$2D_{aO_2{}^+}\frac{l_p}{{l_2}^2} = \left(1 - \frac{{l_p}^2}{{l_2}^2}\right)u_{BO_2{}^+} . \quad (27)$$

Similarly, for the O^+ ions, we have

$$2D_{aO^+}\frac{l_p}{{l_1}^2} = \left(1 - \frac{{l_p}^2}{{l_1}^2}\right)u_{BO^+} . \quad (28)$$

Thus, l_1 and l_2 can be obtained. From Eq. (24), the positive-ion density at $x = l$ (electronegative core length) is written as

$$n_{O_2{}^+}(l) = n_2\left(1 - \frac{l^2}{{l_2}^2}\right) . \quad (29)$$

Then, solving Eq. (29) for n_2 gives

$$n_2 = \frac{n_{O_2{}^+}(l)}{\left(1 - \frac{l^2}{{l_2}^2}\right)} . \quad (30)$$

Similarly, for the O^+ ions, we have

$$n_1 = \frac{n_{O^+}(l)}{\left(1 - \frac{l^2}{{l_1}^2}\right)} . \quad (31)$$

2. Flat-Top Model

We assume a flat-top distribution of negative ions and positive ions in the $l_p - d < x < l_p$ region and a constant electron density over the entire range $(0 < x < l_p)$ as

$$n_{O_2^+}(x) = \overline{n_{O_2^+}} \left(1 - \frac{(x-(l_p-d))^2}{d^2}\right) + n_{O_2^+}(l_p-d) , \quad (32)$$

$$n_{O^+}(x) = \overline{n_{O^+}} \left(1 - \frac{(x-(l_p-d))^2}{d^2}\right) + n_{O^+}(l_p-d) , \quad (33)$$

$$n_-(x) = n_{e0}\alpha_0 \left(1 - \frac{(x-(l_p-d))^2}{d^2}\right) , \quad (34)$$

where d is the width of the non-flat region; the profiles are shown in Fig. 2(b).

In the region $x < l_p - d$, profiles of the positive-ion density and the negative-ion density are flat. Then, the equations for the positive-ion particle balance are

$$k_{iz2} n_{O_2} n_e l_p = k_{rec2} \overline{n_{O_2^+}} \alpha_0 n_e \left(l_p - \frac{7}{15}d\right) + \frac{2}{3} k_{rec2} n_{O_2^+}(l) \alpha_0 n_e \left(l_p - \frac{1}{3}d\right) + \frac{2 D_{aO_2^+} \overline{n_{O_2^+}}}{d} , \quad (35)$$

$$k_{iz1} n_O n_e l_p = k_{rec1} \overline{n_{O^+}} \alpha_0 n_e \left(l_p - \frac{7}{15}d\right) + \frac{2}{3} k_{rec1} n_{O^+}(l) \alpha_0 n_e \left(l_p - \frac{1}{3}d\right) + \frac{2 D_{aO^+} \overline{n_{O^+}}}{d} . \quad (36)$$

The particle-balance equation for negative ions can be written as

$$\begin{aligned} k_{att} n_{O_2} n_e l_p = {} & k_{rec2} \overline{n_{O_2^+}} \alpha_0 n_e \left(l_p - \frac{7}{15}d\right) \\ & + k_{rec1} \overline{n_{O^+}} \alpha_0 n_e \left(l_p - \frac{7}{15}d\right) + k_{det} \alpha_0 {n_e}^2 \left(l_p - \frac{1}{3}d\right) \\ & + k_{rec2} \alpha_0 n_e n_{O_2^+}(l) \left(l_p - \frac{1}{3}d\right) \\ & + k_{rec1} \alpha_0 n_e n_{O^+}(l) \left(l_p - \frac{1}{3}d\right) . \end{aligned} \quad (37)$$

For the charge neutrality of the center of the EN core region, we have

$$\overline{n_{O_2^+}} + \overline{n_{O^+}} = \alpha_0 n_e . \quad (38)$$

The ion-flux balance equation in the region $0 < x < l_p - d$ can be written as

$$\frac{2 D_{aO_2^+} \overline{n_{O_2^+}}}{l_p - d} + k_{iz2} n_e n_{O_2} d = h_l n_{O_2^+}(l) u_{BO_2^+} , \quad (39)$$

$$\frac{2 D_{aO^+} \overline{n_{O^+}}}{l_p - d} + k_{iz1} n_e n_O d = h_l n_{O^+}(l) u_{BO^+} . \quad (40)$$

The power-balance equation can be written as

$$\begin{aligned} P_{abs} = {} & \left(k_{iz2} n_e n_{O_2} \varepsilon_{c2} + k_{iz1} n_e n_O \varepsilon_{c1}\right) V \\ & + h_l \left(n_{O_2^+}(l) u_{BO_2^+} n_{O^+}(l) u_{BO^+}\right) (\varepsilon_e + \varepsilon_i) A \end{aligned} \quad (41)$$

Finally, for the charge neutrality at $x = l$, we have

$$n_{O_2^+}(l) + n_{O^+}(l) = n_e . \quad (42)$$

III. RESULTS AND DISCUSSION

Based on the parabolic and the flat-top model equations presented in Sec. , the spatial profile of the charged species, the EN core length l (parabolic model), d (flat-top model), and the electron temperature are calculated. It is found that, over low (1 - 100 mTorr) and medium (100 - 250 mTorr) pressures, the results of the models are in agreement with the experimental results. The analytic models developed here should adequately describe the plasma equilibrium. The ultimate tests of both analytic models are comparisons with experiments. In Figs. 3(a) and 3(b) for pressures of 70 mTorr and 100 mTorr respectively, we show the density profiles calculated for the four species by using the parabolic model, Eqs. (5) - (6) and Eqs. (13) - (21) with an input power of 200 W and a γ_{rec} of 0.1. These eight algebraic equations of the parabolic model are solved numerically by using the Gauss-Jordan elimination. The electronegative core length is highly pressure dependent. In Figs. 4(a) and 4(b) for medium pressures of 170 mTorr and 250 mTorr respectively, we show the density profiles calculated at an input power of 200 W and a γ_{rec} of 0.1 by using the flat-top model, Eqs. (5) - (6) and Eqs. (35) - (42). These eight algebraic equations of the flat-top model are solved numerically by the same method as above. As the pressure increases, the electronegative core length and α_0 also increase, and the volume recombination loss mechanism becomes more important. The profiles obtained by the two models are compared well with other simulation results and experiments, giving reasonable agreement [16].

The behavior of the electron temperature as a function of the input power is shown in Fig. 5. Figure 5 indicates good agreement between the present analysis and the experimental data. The prediction of the electron temperature being a weak function of power is confirmed by the experimental measurements [19]. The comparison between the experiment and the model shows qualitative agreement. However, the agreement is not quantitative. Figure 6 shows an acceptable agreement between the experimental results which indicate a monotonically decreasing positive-ion density [20] and the results of our model. Figure 7 shows the variation of the negative-ion density as a function of the pressure. The experimental results show a reasonable agreement with our one-dimensional equilibrium model predictions [21]. The electron density is about $10^{17} - 10^{18}$ m^{-3}, and the negative-ion density about five to ten times higher. The dominant negative-ion, O^-, is produced by dissociative attachment and pair production of O_2 and is destroyed

by ion-ion recombination and detachment at low pressures. The competition between ion-ion recombination and detachment explains the peak in the negative-ion density. At low pressure (below 25 mTorr), the O^- balance is governed by dissociative attachment to O_2 and ion-ion recombination. The densities of the negative ions and O^+ increase with pressure. On the other hand, recombination and detachment become dominant at pressures above 25 mTorr, resulting in a decrease of the negative-ion density. The competition between these destruction processes results in a maximum density at about 25 mTorr.

IV. CONCLUSIONS

We have developed a parabolic and a flat-top model, applicable to low and medium pressure (1 - 250 mTorr) electronegative oxygen discharges, and the plasma profile can be specified in both models. One-dimensional algebraic particle- and power-balance equations were written for both neutral and charged species. The charged and the neutral particle densities, together with the electron temperature, were calculated with the rf power, the inlet pressure, the reactor diameter, and the reactor length as input discharge parameters. The results showed that the dominant positive-ion is ${O_2}^+$ rather than O^+.

The dependences of the electron temperature and the ion density on the power and the pressure were in qualitative agreement with experimental results. For a typical oxygen discharge of $p = 100$ mTorr and $P_{abs} = 200$ W, the result showed that the discharge was highly electronegative with a value of $\alpha_0 = n_{O^-}/n_e$ greater than 10 and that the fractional dissociation of oxygen molecules ($\frac{O}{O_2+O}$) was less than 0.1. The present model can also be applied in the highly dissociative region which is widely used in the semiconductor industry.

ACKNOWLEDGMENTS

This work is supported by Dong-A University and by the Basic Science Research Institute Program, Korea Ministry of Education (BSRI-97-2439).

REFERENCES

[1] C. Lee and M. A. Lieberman, J. Vac. Sci. Technol. **A13**, 368 (1995).
[2] S. K. Park and D. J. Economou, J. Appl. Phys. **68**, 3904 (1990).
[3] T. J. Sommerer and M. J. Kushner, J. Vac. Sci. Technol. **B10**, 2179 (1992).
[4] N. S. Yoon, S. S. Kim, C. S. Chang and Duk-In Choi, J. Korean Phys. Soc. **28**, 172 (1996).
[5] M. Yoon, S. C. Kim, H. J. Lee and J. K. Lee, J. Korean Phys. Soc. **32**, 635 (1998).
[6] Y. T. Lee, M. A. Lieberman, A. J. Lichtenberg, F. Bose, H. Baltes and R. Patrick, J. Vac. Sci. Technol. **A15**, 113 (1997).
[7] M. A. Lieberman and S. Ashida, Plasma Sources Sci. Technol. **5**, 145 (1996).
[8] J. T. Gudmundsson and M. A. Liberman, Plasma Sources Sci. Technol. **7**, 1 (1998).
[9] A. J. Lichtenberg, V. Vahedi, M. A. Lieberman and T. Rognlien, J. Appl. Phys. **75**, 2339 (1994).
[10] I. G. Kouznetsov, A. J. Lichtenberg and M. A. Lieberman, Plasma Sources Sci. Technol. **5**, 662 (1996).
[11] A. J. Lichtenberg, I. G. Kouznetsov, Y. T. Lee, M. A. Lieberman, I. D. Kaganovich and L. D. Tsendin, Plasma Sources Sci. Technol. **6**, 437 (1997).
[12] T. H. Chung and H. J. Yoon, J. Korean Phys. Soc. **31**, 364 (1997).
[13] G. A. Hebner, J. Appl. Phys. **81**, 578 (1997).
[14] T. Mieno, T. Kamo, D. Hayashi, T. Shoji and K. Kadota, Appl. Phys. Lett. **69**, 617 (1996).
[15] C. K. Birdsall, IEEE Trans. Plasma Sci. **19**, 65 (1991).
[16] T. H. Chung, L. Meng, H. J. Yoon and J. K. Lee, Jpn. J. Appl. Phys. **36**, 2874 (1997).
[17] T. H. Chung, H. S. Yoon and J. K. Lee, J. Appl. Phys. **78**, 6441 (1995).
[18] M. A. Lieberman and A. J. Lichtenberg, *Principles of Plasma Discharges and Materials Processing* (Wiley, New York, 1994).
[19] J. E. Heidenreich and A. R. Paraszczak, J. Vac. Sci. Technol. **B6**, 288 (1988)
[20] J. H. Keller, J. C. Forster and M. S. Barnes, J. Vac. Sci. Technol. **A11**, 2487 (1993)
[21] E. Stoffels, W. W. Stoffels, D. Vender, M. Kando, G. M. W. Kroesen and F. J. de Hoog, Phys. Rev. **E51**, 2425 (1995).